A MESH BASED BOOM TO STOP OIL SPREAD

By

Bharathram Visweswaran, B. E.

A Thesis Presented in Partial Fulfillment
of the Requirements for the degree
Master of Science in Engineering

COLLEGE OF SCIENCE AND ENGINEERING
UNIVERSITY OF TEXAS, ARLINGTON

May 2016

ABSTRACT

In this work, we develop a new boom to separate oil and water. In a commonly used boom, a membrane that has no pores is normally used to block oil spread. Since this membrane also blocks water flow, high pressure is easy to build on such a membrane to break or damage it. To solve this problem, in the new boom, the membrane is replaced with a hydrogel-coated mesh. The hydrogel-coated mesh has dual properties of superhydrophilicity and superoleophobicity. Accordingly, water can still go through the mesh, while oil cannot. Subsequently, liquid pressure on the mesh is reduced. In this work, we explore the development of the new boom.

TABLE OF CONTENTS

LIST OF TABLES

LIST OF FIGURES

ACKNOWLEDGEMENTS

I would like to express my sincere gratitude and thanks to my research advisor, Dr. Cheng Luo, for his constant support and guidance during my research at University of Texas, Arlington. My special thanks go to him for teaching me the importance of having the positive attitude to life, which has benefitted me much more than the research techniques I obtained during my graduate studies. I would like to thank Dr. Jeyjin Moon and Dr. Zhen Xue Han for their support, for their suggestions in perfecting the thesis, and for agreeing to be in my graduate committee.

My group members, Mr. Manjarik Mrinal, Mr. Mithun Rajaram and Mr. Manasvi Oza, deserve special mentioning for their co-operation and continuous support. Long hours of discussion and debates with them were very helpful and were the source of many new ideas. My friend, Manjarik Mrinal, was always encouraging me and willing to share his precious experiences with me. I give special thanks to him.

I thank my family and the almighty, for their support and belief, which has enabled me to accomplish my academic pursuits.

CHAPTER 1

INTRODUCTION

1. Overview of Virtual Wall and Oil Dam Techniques

Due to the fact that oil-based compounds are referred to as low-surface tension liquids, they tend to spread on the surface where the liquids are placed. Accordingly, as can be seen from oil spills in the Gulf of Mexico in the last few years [1-4], oil can stick and easily spread out on any surface. Oil spills are a very dangerous occurrence for marine ecosystem [1,3,4]. Since exploration of oil from oceanic resources has become a must and oil spills end up occurring accidently, as a result, some techniques have been developed to block oil spreading [5-7]. For example, researchers have developed an oil-repellant surface to form a so-called “virtual” wall for oily liquids that may help confine them to a certain area [5]. However, it involves much effort to fabricate such a well through deposition and etching processes. In addition, some engineers have come up with an idea that is to plug the leak by placing a giant dome over it [5]. Subsequently, the dome would stop the oil and then pump the oil into tanks on the surface. However, preparing the giant dome could take several months to complete. Moreover, oil booms are a widely used method of controlling oil spills [7]. The booms function as dams to stop oil spreading. A typical oil boom includes freeboard, skirt, and ballast (Fig. 1a) [8]. The freeboard is extended above water surface to prevent oil from being washed over the boom. Skirt is the continuous portion of the freeboard under water. It is the main component of the boom to block the spread of the oil. Ballast is the weight placed at the bottom of the skirt to make it maintain its vertical orientation. A major concern about an existing skirt is its solid surface. High water pressure is easy to build up on such a

surface to break the skirt [7]. On the other hand, water pressure is not a major concern in the case of fishing nets. Water can go through their pores, resulting in much lower pressure on the nets. Observation of this difference in water pressure motivates a new idea: replace the existing skirt in an oil boom with a mesh for effectively stopping the spread of spilled oil (Figs. 1b and 1c). In this work, we explore this idea.

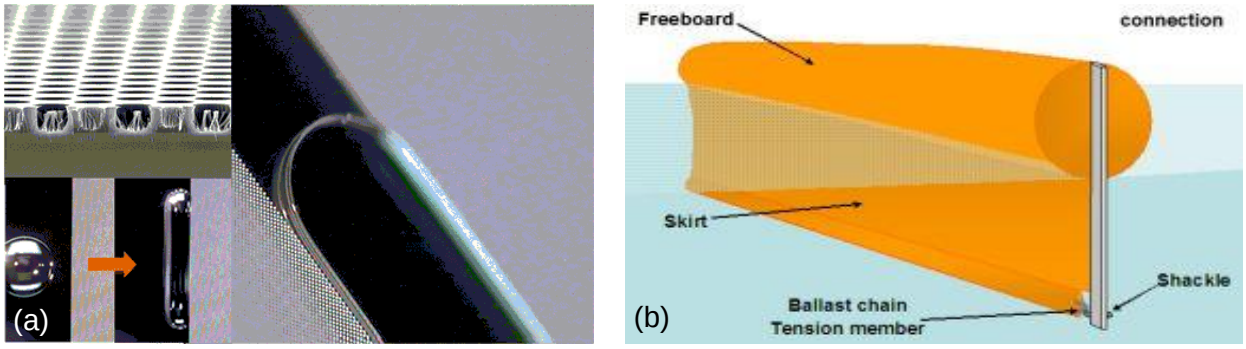

Figure 1.1: Previous research projects of (a) virtual wall [5] and (b) oil boom [8].

CHAPTER 2

DESIGN OF THE MESH

2.1 Two specific requirements about the mesh

In the case of fishing nets, fish is caught due to the fact that its size is larger than a net pore. However, the same does not apply to oil, which is a liquid and may easily deform to go through a mesh pore. Also, generally speaking, since oil has a lower surface tension than water, it tends to wet a surface more easily. This means that it may be easier than water to penetrate a mesh pore. According to these concerns, there are two critical differences between the chosen mesh and fishing nets: (i) the selected mesh is coated with hydrogel, and (ii) it also has smaller pores, whose sizes are in the order of 100 μm. These two differences are also two specific requirements about the mesh. Crude oil has a lower surface tension than water. As a result, crude oil usually forms a smaller contact angle with a solid surface, making the oil much easier than water to penetrate a mesh pore. To solve this problem, hydrogel will be used to cover mesh fibers. Hydrogels are found to have excellent capabilities of absorbing and retaining water. Thus, their coatings may create water films on the mesh surfaces. Consequently, in water bath, crude oil forms a large contact angle with the mesh surface, which is above 150^{o}. In contrast, the contact angle of seawater on such a surface is 0^{o}, since the seawater is contacting itself. Thus, the hydrogel coating should make the chosen mesh have the dual properties of superoleophobicity and superhydrophilicity. Accordingly, water is free to go through the mesh pores, while crude oil does not. Furthermore, a small pore size makes oil difficult to penetrate the pore even under high dynamic pressure. If needed, multiply stacked meshes, for example, can be placed on site to

handle high-speed oil spills. In next two sub-sections, we further discuss the two specific requirements.

2.2. Theoretical modeling

After crude oil contacts a mesh pore which is surrounded by seawater, whether oil can go through the pore depends not only on its contact angle but also on the pore size. A 2-D model is developed to examine the effects of contact angle and pore size. The pores have straight sidewalls, while their corners are round in practice, whose radii are much smaller than the height, width and thickness of a pore. Let θ denote contact angle of crude oil on the surface of a mesh fiber (Fig. 2). Set φ to be the angle between the pore sidewall and mesh surface. Both angles range between 0^{o} and 180^{o}. Use γ to represent surface tension of crude oil. Set *w* to be the distance between two pore sidewalls. Let p_o denote oil pressure in front of the pore, and set p_w to be seawater pressure behind the pore. $(p_o - p_w)$ is so-called Laplace pressure, which in this case represents the difference between the pressures in front of and behind the mesh. Then, we have [14]

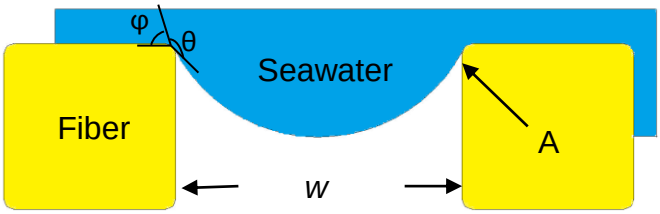

Figure 2.1: Schematic of crude oil at a mesh pore in seawater

$$p_o - p_w = \frac{2\gamma\cos(270^o - \varphi - \theta)}{w}. \quad (1)$$

When θ is larger than 90°, the critical pressure that is needed for crude oil to go through a pore is $(p_o - p_w)_{cri} = \frac{2\gamma\cos(180^o - \theta)}{w}$, which occurs when the oil/water interface is located between the lowest points of the two top corners of the pore (such a point is marked as "A" in Fig. 2). It can be observed from this relation that $(p_o - p_w)_{cri}$ increases with both the increase in θ and the decrease in *w*. For crude oil with γ of 35 mN/m and θ of 150° (i.e., the mesh is superoleophobic) and *w* of 100 μm, $(p_o - p_w)_{cri}$ should be at 0.61 kPa. The dynamic liquid pressure is

$$p = 0.5\rho v^2, \quad (2)$$

where ρ and *v* denote liquid density and speed, respectively. Therefore, when the spreading speed of crude oil is 1 m/s, *p* is 0.44 kPa, where the density of 873 kg/m^3 for Texas crude oil was used in the calculation. Thus, a mesh with 100 μm pores is good enough to stop the spread of oil with a speed of 1 m/s or less. Subsequently, the pores in the proposed mesh are designed to have sizes in the order of 100 μm. In case the spreading speed is higher than 1 m/s, there are still two solutions. The first one is to place multiply stacked meshes on site. The spreading speed of the oil is gradually reduced after the oil goes through the meshes one by one, and should be finally stopped when its speed is reduced to 1 m/s or less. The second solution is to further reduce the pore size. For example, when the pore size is reduced to 10 μm, $(p_o - p_w)_{cri}$ is increased to 6.1 kPa. Therefore, a single mesh is good enough to block the spread of oil with a speed less than 3.8 m/s.

If crude oil in Fig. 2 is replaced with seawater and also if the contact angle of seawater on the mesh surface is 0° (i.e., the mesh is superhydrophilic), it follows from

Eq. (1) that the critical pressure is zero. Accordingly, the seawater in the incoming flow can penetrate a pore without any obstacles. In summary, the spread of crude oil should be stopped by a mesh, which has dual properties of superoleophobicity and superhydrophilicity and which also has small pores.

Based on the requirement of 100μm level meshes, we chose 4 different meshes shown in Figure which are 304μm, 140μm, 101μm and 80μm meshes and they are coated with 10% concentration hydrogel solution (explained in 3.1 Types of tests). Based on the contact angle of oil, Pore size of the mesh and surface tension of Silicone oil, using Eq.1, the $P_{ocritical}$ was found for each mesh. And by using the $P_{ocritical}$ value calculated from Eq.1, using Eq.2, the $V_{ocritical}$ has also been found for each mesh inorder to match these velocity values with the experimental velocity values.

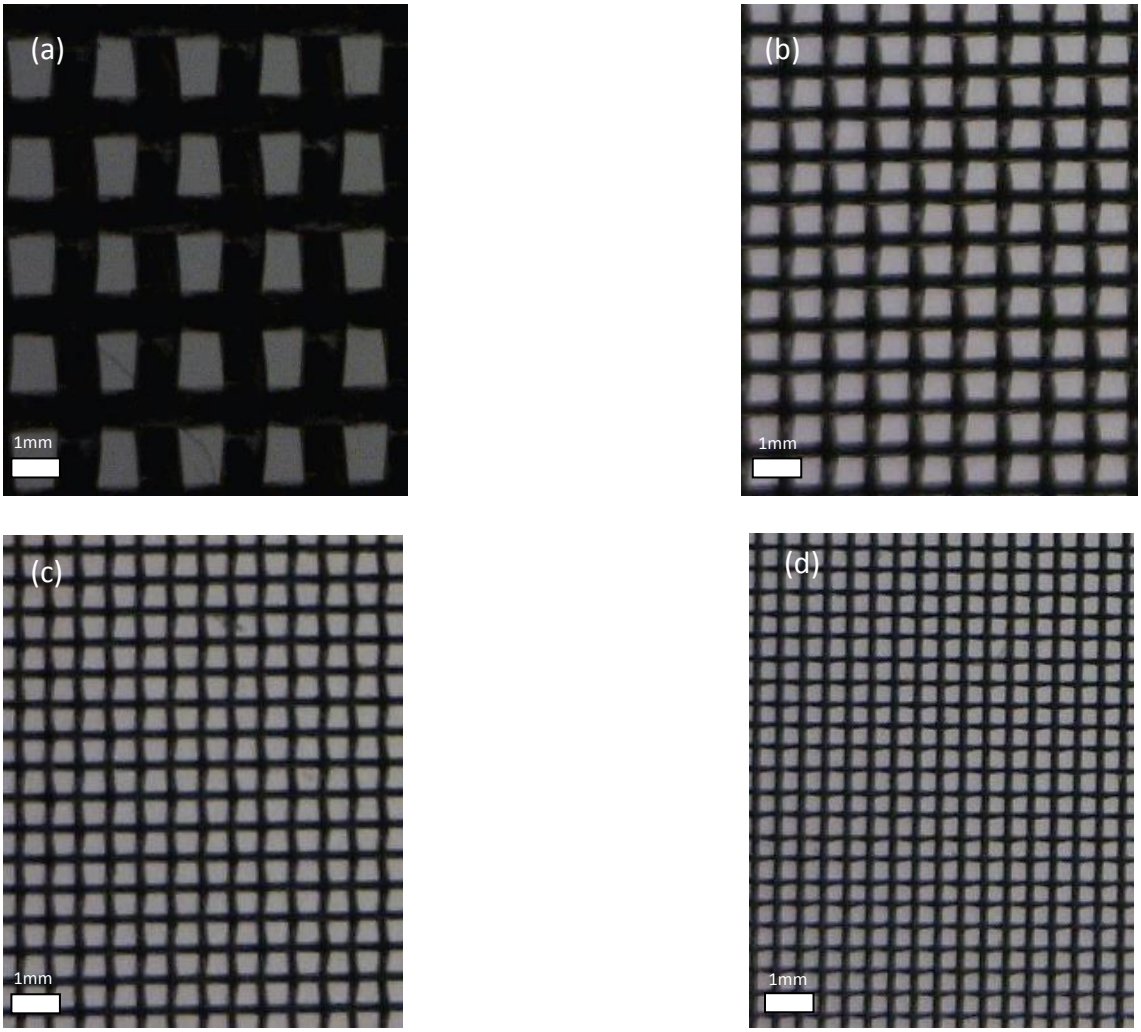

Figure 2.2: Four different pore size meshes which are (a) 304μm, (b) 140μm, (c) 101μm and (d) 80μm, respectively.

Mesh Size (μm)	**Contact angle (deg)**	**$P_{ocritical}$ (kPa)**	**$V_{critical}$ (m/s)**
304	128.5	0.14	0.29
140	148.3	0.43	0.94
101	148.6	0.59	1.22
80	148.9	0.75	1.54

Table 2.1: Theoretically calculated values of critical pressure and velocities.

2.3. Superoleophobicity and superhydrophilicity

The degree that a surface repels a liquid increases with contact angle of this liquid. The contact angle of a liquid on a surface can be determined using well-known Young-Dupré equation [15]:

$$\cos\theta = \frac{\gamma_{SA} - \gamma_{SL}}{\gamma}, \quad (2)$$

where γ_{SL} and γ_{SA} denote surface tensions of solid/liquid and solid/air interfaces, respectively. At 24 ºC, γ of crude oil ranges from 25.6 to 45.8 mN/m, depending on the type of crude oil and the measurement approaches [16]. At the same temperature, γ of seawater varies from 74 to 78 mN/m for a salinity range of 10 to 35 g/kg [17]. Hence, seawater has a larger γ than crude oil. Furthermore, γ_{SL} for seawater is generally larger than that for crude oil. Hence, for the same solid surface, i.e., for the same γ_{SA}, the right-hand side of Eq. (2) for seawater is smaller than that for crude oil, indicating that seawater has a higher contact angle than crude oil. Accordingly, it is easy to design a solid surface which is more repellent to seawater. However, the proposed mesh should be more repellent to crude oil.

Large contact angle of oil is generated when the following two conditions are met: (i) the solid surface is covered by a seawater film, and (ii) the oil is surrounded by seawater. Subsequently, (a) γ_{SL} in Eq. (2) becomes the interfacial tension between seawater and seawater, which is 0, (b) γ_{SA} is replaced with the interfacial tension between crude oil and seawater, and (c) γ is also changed to the interfacial tension between crude oil and seawater. Hence, by Eq. (2), we have $\cos\theta$=-1, implying that, in this case, the oil drop has a contact angle of about 180º on a surface that is covered by a seawater film. Meanwhile, it is obvious that the contact angle of seawater on a

seawater-covered surface is 0^{o}. Consequently, the corresponding surface is superoleophobic to oil but superhydrophilic to water.

Hydrogels are found to have excellent capabilities of absorbing and retaining water. Thus, they are chosen as coating materials to create water films on the surfaces of the mesh. On the other hand, when the oil is also exposed to air, its contact angle is reduced. Therefore, the top portion of the mesh should be solid to block the spread of the oil, and the pores are only included in the bottom portion of the mesh that are submerged in sea.

CHAPTER 3

EXPERIMENTAL RESULTS AND DISCUSSIONS

3.1 Two Types of Tests

As observed from Eq. (1), the maximum liquid pressure that is needed for oil to penetrate a pore increases with the decrease in the pore size. Pore sizes have been selected to be 100 μm. Silicone oil and purified water have surface tensions of 35 [18] and 72 mN/m [15], respectively. The surface tension of silicone oil is close to the average value of the surface tensions reported for crude oil, while purified water and sea water have similar surface tensions. Therefore, in our tests, silicone oil and purified water are chosen, respectively, as the representatives of crude oil and seawater. Three types of tests have been done to examine different aspects of the mesh.

In the first type of experiments, we examined contact angles of water and oil on different coatings. As shown in Figs. 4(a1) and (a2), purified water and silicone oil have contact angles of 53^o and 1^o, respectively, on SiO_2-coated Si plates. Furthermore, as given in Figs. 5(a1) and (a2), purified water and silicone oil have contact angles of 130^o and 10^o, respectively, on Teflon-coated steel meshes. Both results validate the theoretical prediction that crude oil has a smaller contact angle on a solid surface than seawater. Thus, the corresponding mesh cannot be applied to stop the spread of spilled oil, since the crude oil is easier to penetrate the mesh pores than seawater. However, as shown in Fig. 4(b1), the contact angle of silicone oil on a SiO_2-coated Si plate was increased from 1^o in air to 30^o in water bath. This contact angle was further increased to 166^o, when the SiO_2-coated Si plate was coated with gelatin hydrogel (Fig. 4(b2)). Also,

in water bath, the contact angles of silicone oil on stainless steel meshes that were coated without and with gelatin hydrogel are 101^{o} and 167^{o}, respectively (Figs. 4(b1) and (b2). These results also validate the theoretical prediction that, in water bath, the hydrogel coating on a surface can make the corresponding surface superoleophobic.

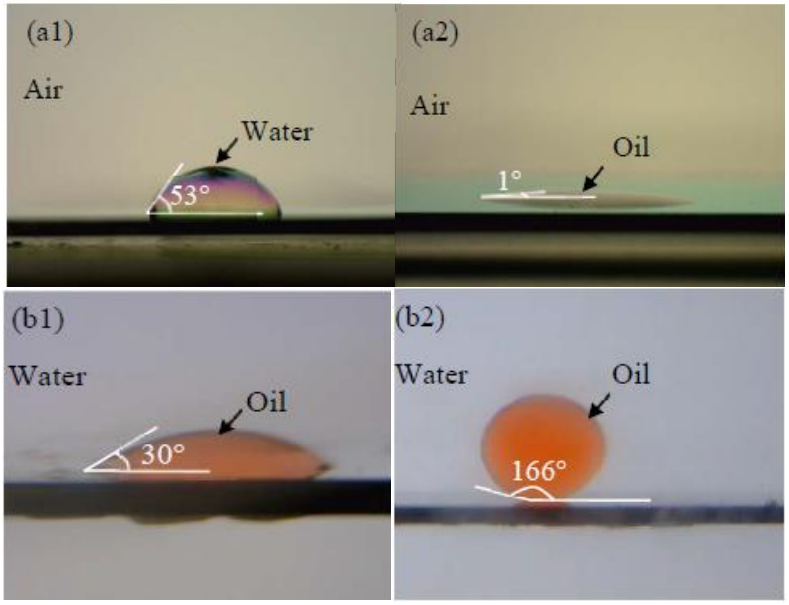

Figure 3.1: In air, (a1) purified water and (a2) silicone oil drops on SiO_2-coated Si plates. In water bath, silicone oil drops on the same plates (b1) without and (b2) with hydrogel coatings.

In the second type of experiments, which includes two tests, we examine whether gelatin hydrogel-coated meshes could be applied to block oil spread. In the first test of this type, a gelatin hydrogel-coated mesh was first immersed in water bath, and silicone oil drops were then injected into the locations under the mesh (Fig. 5(c1)). An oil drop moved up, since it was less dense than water. However, its movement was stopped by the mesh (Fig. 5(c2)). Likewise, all the injected silicone oil drops were blocked by the mesh (Figs. 5(c3) and (c4)). The results of the first test demonstrate the feasibility of applying a hydrogel-coated mesh to stop oil spreading.

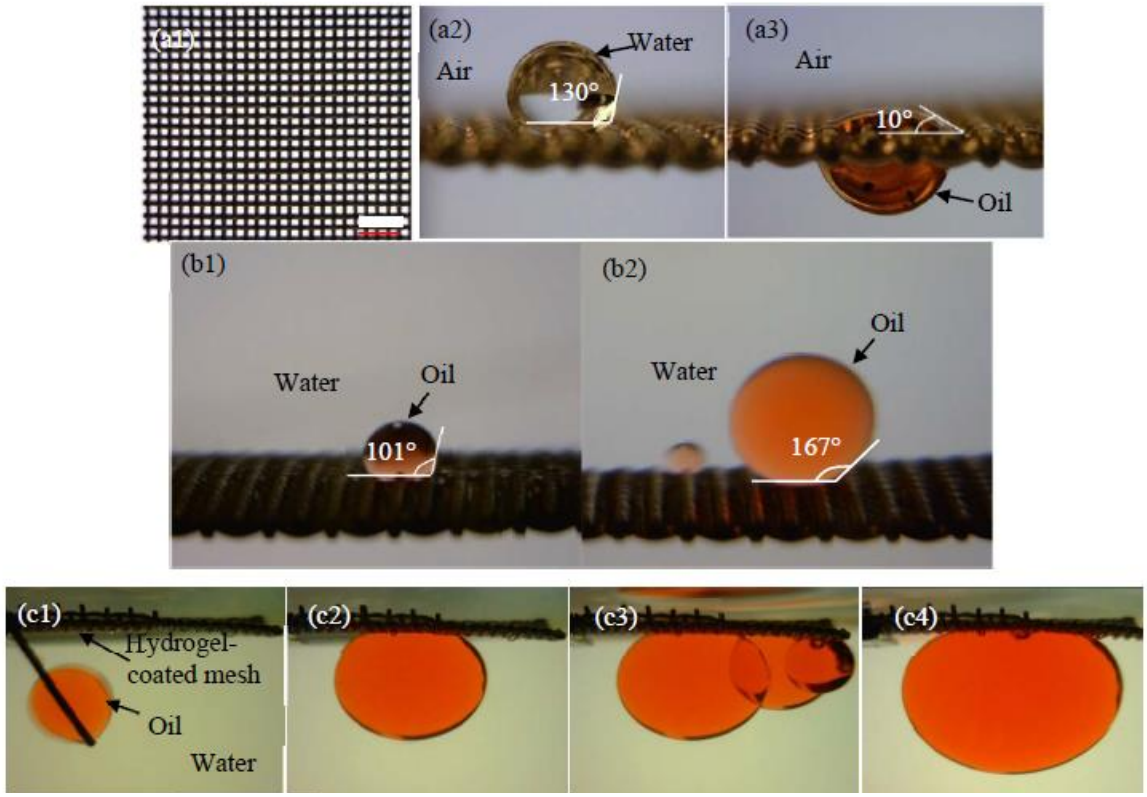

Figure 3.2: (a1) Top view of a stainless steel mesh with pore size of 304 µm and fiber diameter of 343 µm (scale bar represents 2 mm). Side views of (a2) water and (a3) silicone oil drops on the Teflon-coated mesh. In water bath, silicone oil drops on stainless steel meshes (b1) without and (b2) with hydrogel coatings. (c) The hydrogel-coated mesh blocked the oil spread: (c1) immerse the mesh in the water bath, and inject silicone oil drops under the mesh, and (c2-c4) the oil drops could not

Based on the above second type of experiment, as already explained 4 different meshes such as the 304µm, 140µm, 101µm and 80µm, we coated with 3 different concentrations of hydrogel coatings such as the 5%, 10% and 15% to analyse the particular concentration feasible for the mesh to stop oil spread. These concentrations are prepared by mixing the porcine powder and water in the ratios of 5:1 for 5% concentration, 10:1 for 10% concentration and 15:1 for 15% concentration. For example, preparing 5% concentration hydrogel solution, we mix 5ml of porcine powder to 1ml of water. The reason for using porcine powder is because of its biocompatibility with water. The meshes are coated with these concentrations of hydrogel solutions and immersed in water bath and add oil droplets over it and checked the contact angle of oil

shown in Figure 6. Based on the contact angle of oil over the mesh, we came to a conclusion that 10% concentration hydrogel solution is the best feasible solution through the analysis shown in Figure 7. Since 5% concentration hydrogel solution gives a lower contact angle and 15% concentration hydrogel solution gives the fluctuation in the contact angles of the oil, hence 10% concentration hydrogel solution is taken into consideration as the feasible solution because it gives a steady increase in the contact angle of oil as the pore size decreases from 304µm to 80µm meshes.

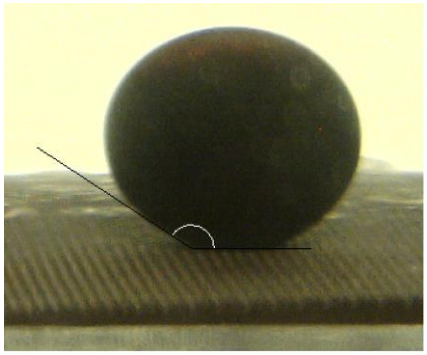

Figure 3.3: Measurement of contact angle of oil over the hydrogel solution coated mesh in underwater.

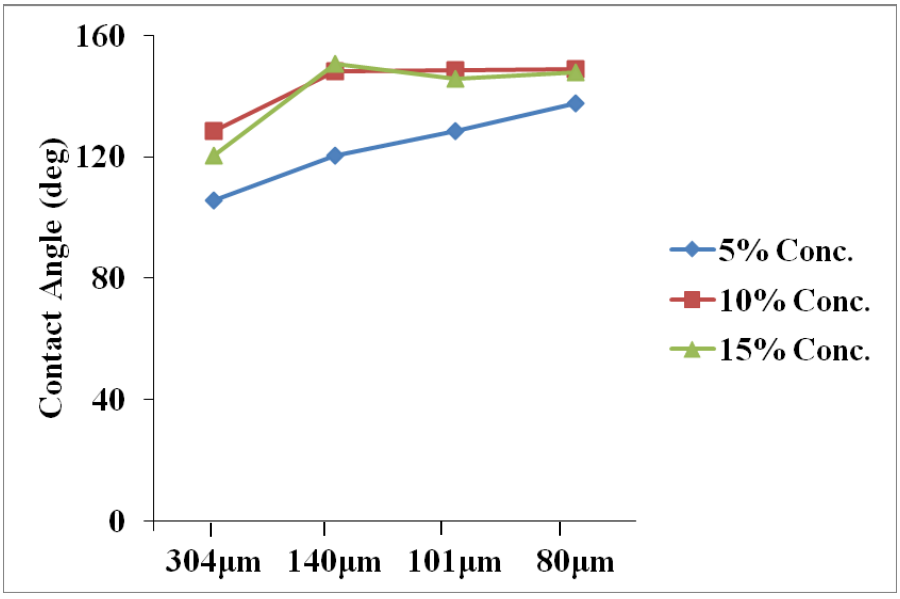

Figure 3.4: Analysis of choosing the best concentration of hydrogel solution based on the contact angle of oil over the hydrogel solution coated mesh.

3.2 Experimental Setup of Dynamic Oil Flow

Based on the understanding gained from the first two types of tests, we conducted the third type of tests, which was to simulate the real situation of stopping oil spread. Figures 8(a) and (b) are the experimental and the illustration setups of the dynamic flow experiment. The setup is of the dimension 3.5 inch X 12 inch (width X height) and the mesh used is of the dimension 3.5 inch X 3.5 inch which is vertically placed inside the chamber. The setup is made out of acrylic material. The inlet is in the middle of the chamber while the outlet is 1 inch above the centre of the chamber. The inlet source has a “T” connection in which one end of the source is connected to the chamber while the other end is connected to the plunger chamber. Along with the inlet source pipeline to the chamber an oil pipeline is connected.

Experimental Setup

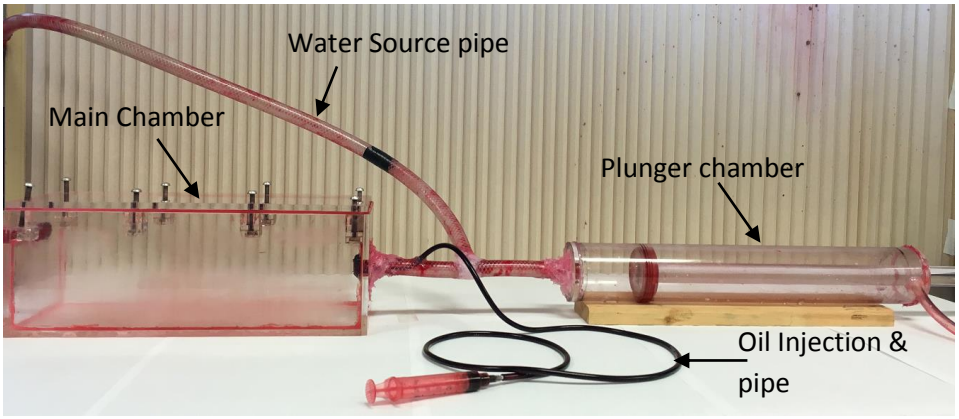

(b)

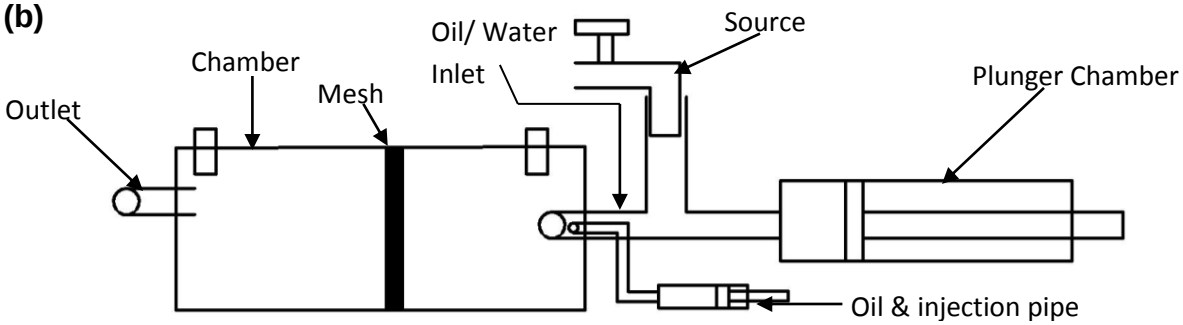

FIGURE 3.5: (a) Experimental setup of the dynamic flow, and (b) Its Illustration.

(a)

3.3 Flow patterns

Firstly the mesh is placed in the middle of the chamber and the water is made to fill the chamber from the water source. After filling the whole mesh with water, the oil is being injected along with the water flow. After injecting oil along with the water flow, oil droplets are formed and moves in the pattern of water flow. Through that movement, the oil flow pattern is judged. The oil droplets can either bounce back without penetrating through the mesh or penetrate through the mesh and flows out of the chamber through the chamber outlet. Figures 9 (a) and (b) shows the experimental and illustrated views of the flow pattern of oil in the chamber. The mesh used in the experiment, shown in Fig.7(a) is 140 μm pore size. With the inlet of the water, the oil is injected along with the water flow. Based on the velocity of the water, the oil droplet moves towards the mesh. The path taken by the droplet in the images is a circular path and it did not penetrate through the mesh as the dynamic liquid pressure of the oil is lesser than the threshold pressure value, which was 0.43 kPa. With the increase of the force, liquid speed also gradually increased. We found the threshold speed for the oil to penetrate the mesh pores, which by Eq. (2) indicated that the threshold pressure was 0.43 kpa**.** The determined threshold pressure was close to the value predicted using Eq. (1), which was 0.43 kPa.

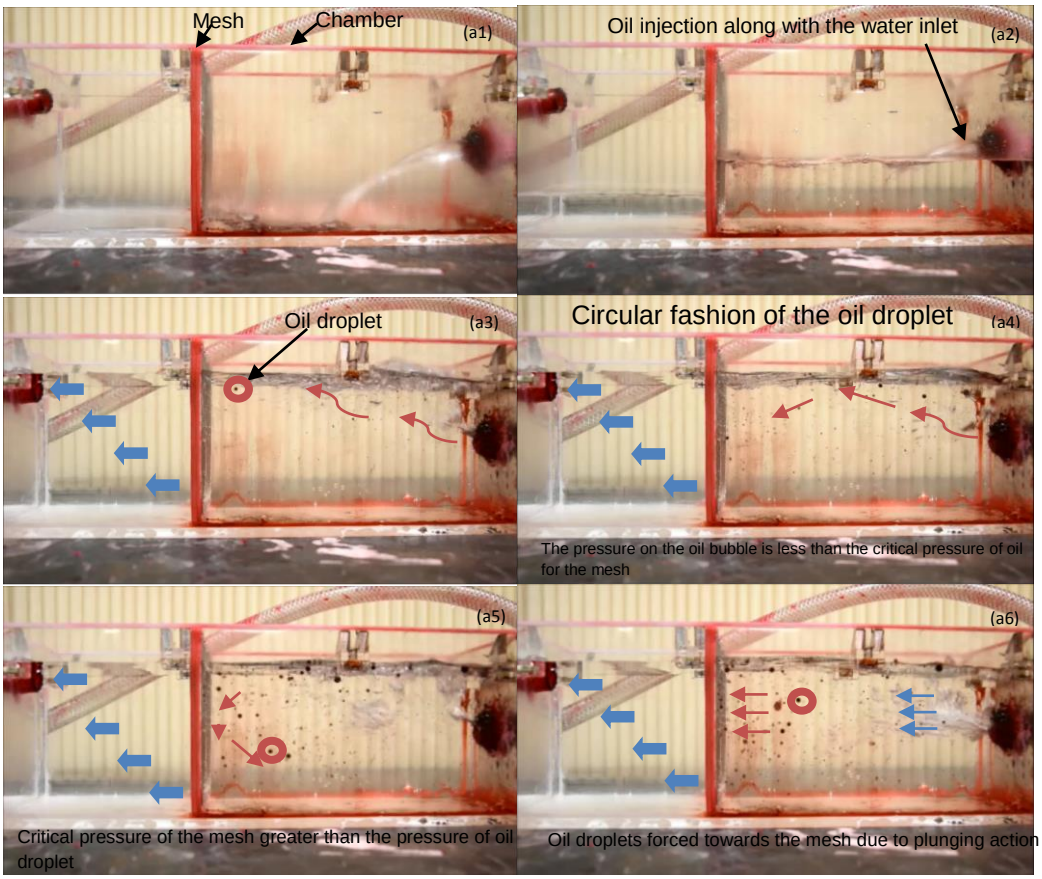

Illustrated view

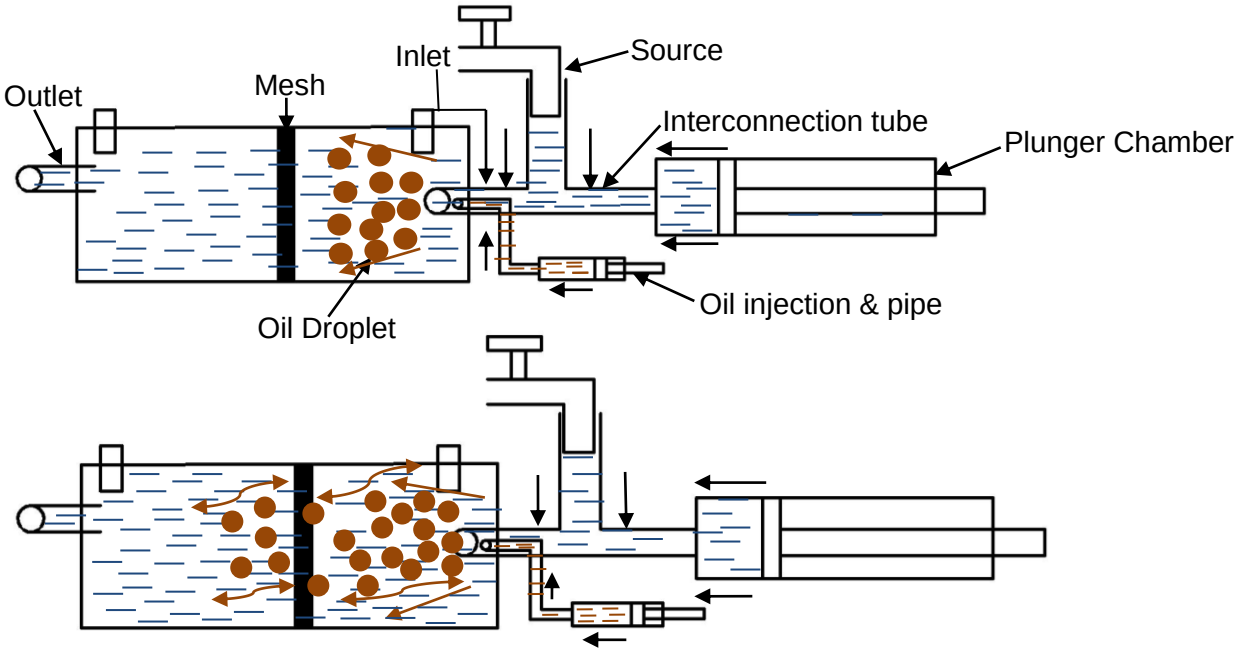

FIGURE 3.6: (a) Experimental, and (b) illustrated views of the oil flow patterns.

3.4 Experimental Analysis

. The theoretically calculated values, in Table 1, have to be compared with the experimental values and check the penetration of oil through the meshes. For the experimental part, 6 different velocities of water have been taken from the source by using anemometer in Fig. 10 and used those velocities. In this experiment, 4 different meshes such as 304µm, 140µm, 101µm and 80µm coated with 10% concentration hydrogel solution are used. Experiments are conducted for all the 4 meshes by using 6 velocities and found the penetration capability of oil through the meshes. These experimental penetration results are compared with the $V_{critical}$ values calculated by using Eq.2 from Table 1 and found to be matching. Hence the expected results are achieved by comparing with the $V_{critical}$ values.

Mesh Size (µm)	**Contact Angle (deg)**	**V Critical (m/s)**	**Velocity/ oil penetration status (m/s)**					
			V= 0.46	**V=1.06**	**V=1.23**	**V=1.56**	**V=1.95**	**V=2.15**
304	128.5	0.29	Yes	Yes	Yes	Yes	Yes	Yes
140	148.3	0.94	No	Yes	Yes	Yes	Yes	Yes
101	148.6	1.22	No	No	Yes	Yes	Yes	Yes
80	148.9	1.54	No	No	No	No	Yes	Yes

Table 3.1: The oil penetration status of the meshes by comparing the actual $V_{critical}$ of the mesh with the velocity exhibited by the oil in the experiment

Figure 3.7: Anemometer for calculating the velocity

3.5 Oil Droplet Size Analysis

Velocity (m/s)	Oil Droplet size, D (μm)		
	Min. Value	Avg Value	Max Value
0.46	160	240	296
1.06	143	210	287
1.23	133	180	268
1.56	134	150	174
1.95	77	100	156
2.15	74	80	90

Table 3.2: Oil droplet size variations to different velocities of water.

In the above conducted experiment, six different velocities of water are chosen for the experiment and checked the oil penetration through the meshes of different pore sizes.

The penetration status of oil at different velocities through different pore size meshes are found to be matching with theoretical $V_{critical}$ values. An attention has to be forseen on the oil droplet size for the determination of penetration of oil through the mesh. Due to their speeds, the oil droplets which have the sizes greater than the pore size of the mesh bounce back from the mesh, instead of penetrating through the mesh. The lower the water speed, the larger oil droplet size and the higher the droplet speed. The reason behind the reduction of the size of an oil droplet is because of increase in the water speed, which makes the oil droplet to disperse into small sizes. Thus, based on the oil droplet size, the penetration of the oil through a particular pore size happens. Table 3.2, explains the maximum, average and minimum values of the oil droplet sizes for six different velocities of water used in the experiment. Figure 3.8 shows the droplet size reduction accordingly to different velocities.

(a1) 0.46m/s

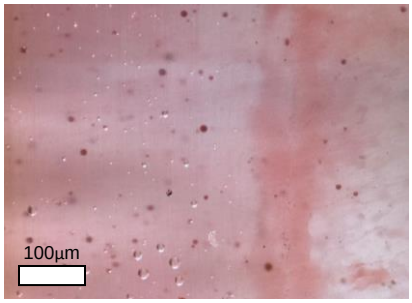

(a2) 1.06 m/s

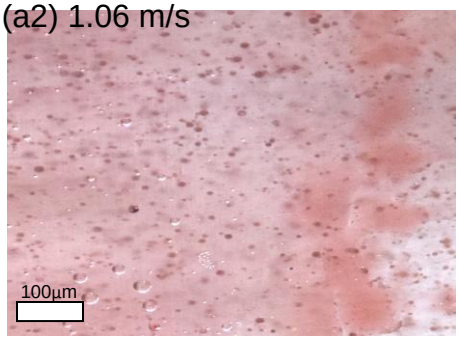

(a3) 1.23 m/s

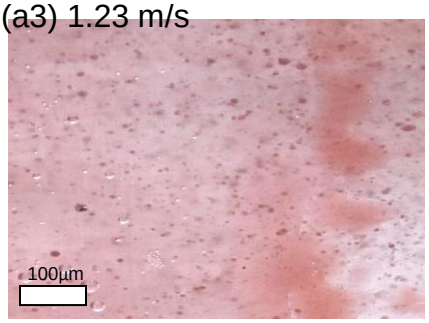

(a4) 1.56 m/s

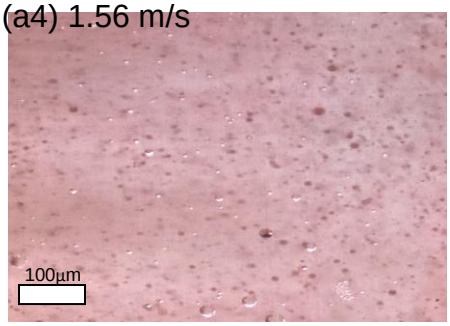

(a5) 1.95 m/s

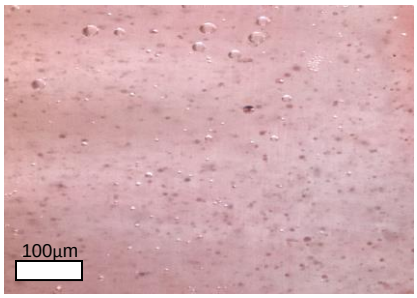

(a6) 2.15 m/s

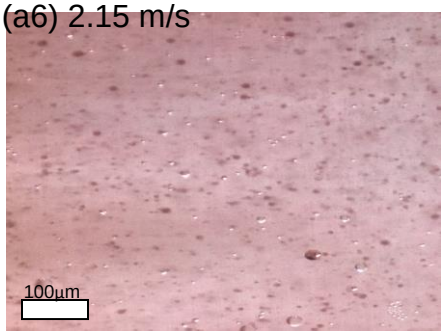

Figure 3.8: (a1) – (a6):Various oil droplet sizes in water bath at six different water speeds before the oil drops strike the mesh.

CHAPTER 4

Summary and conclusions

In this work, we developed a new boom, which replaced the membrane in the existing boom with a mesh. Through theoretical modeling and three types of experiments, we have demonstrated: (i) hydrogel-coated meshes are both superoleophobic and superhydrophilic, and (ii) such meshes could be applied to stop oil spread. In conclusion, the presented results have demonstrated that it is promising to apply the new boom to control the spreading of oil spills.

REFERENCES

1. H. K. White, P.-Y. Hsing, W. Cho, T. M. Shank, E. E. Cordes, A. M. Quattrini, R. K. Nelson, R. Camilli, A. W. Demopoulos, C. R. German, Impact of the Deepwater Horizon oil spill on a deep-water coral community in the Gulf of Mexico. *Proc. Natl. Acad. Sci.* 201118029 (2012).
2. Q. Lin, I. A. Mendelssohn, Impacts and recovery of the Deepwater Horizon oil spill on vegetation structure and function of coastal salt marshes in the northern Gulf of Mexico. *Environ. Sci. Technol.* **46**, 3737-3743 (2012).
3. S. E. Allan, B. W. Smith, K. A. Anderson, Impact of the Deepwater Horizon oil spill on bioavailable polycyclic aromatic hydrocarbons in Gulf of Mexico coastal waters. *Environ. Sci. Technol.* **46**, 2033-2039 (2012).
4. J. E. Kostka, O. Prakash, W. A. Overholt, S. J. Green, G. Freyer, A. Canion, J. Delgardio, N. Norton, T. C. Hazen, M. Huettel, Hydrocarbon-degrading bacteria and the bacterial community response in Gulf of Mexico beach sands impacted by the Deepwater Horizon oil spill. *Appl. Environ. Microbiol.* **77,** 7962-7974 (2011).
5. R. Almeida, J. W. Kwon, Virtual Walls Based on Oil-Repellent Surfaces for Low-Surface-Tension Liquids. *Langmuir* **29**, 994-998 (2013).
6. G. V. Howell, R. Miller, G. Rushbrook-House, A little bird told me: birdcaging the message during the BP disaster. *J. Global Scholar Mark. Sci.* **24**, 113-128 (2014).
7. M. Fingas, *The basics of oil spill cleanup* (CRC Press, Boca Raton, FL, ed. 3, 2012).
8. Oil spill solution: http://www.oilspillsolutions.org/booms.htm.
9. A. Momoi, *Fishing net twine and a fishing net made thereof*. Patents US4947727 (1990).

10. J. G. Derraik, The pollution of the marine environment by plastic debris: a review. *Mar. Pollut. Bull.* **44**, 842-848 (2002).
11. E. K. Bolton, Chemical Industry Medal. Development of Nylon. *J. Ind. Eng. Chem.* **34**, 53-58 (1942).
12. Andrew J. Peacock, *Handbook of polyethylene: structures: properties, and applications* (Marcel Dekker, New York, 2000).
13. X. Liu, C. Luo, Fabrication of super-hydrophobic channels. *J. Micromech. Microeng.* **20**, 025029 (2010).
14. C. Luo, M. Xiang, X. Liu, H. Wang, Transition from Cassie–Baxter to Wenzel States on microline-formed PDMS surfaces induced by evaporation or pressing of water droplets. *Microfluid. Nanofluidics* **10**, 831-842 (2011).
15. A. W. Adamson, A. P. Gast, *Physical chemistry of surfaces* (Wiley, New York, 1976).
16. E. H. Harvey, The Surface Tension of Crude Oils. *J. Ind. Eng. Chem.* **17**, 85 (1925).
17. M. H. Sharqawy, J. H. Lienhard, S. M. Zubair, Thermophysical properties of seawater: a review of existing correlations and data. *Desalin. Water Treat.* **16**, 354-380 (2010).
18. F. Barca, T. Caporossi, S. Rizzo, Silicone Oil: Different Physical Proprieties and Clinical Applications. *Biomed. Res. Int.* **2014**, (2014).
19. H. Omidian, K. Park, *Introduction to Hydrogels* in *Biomedical Applications of Hydrogels Handbook* (Springer, New York, 2010).
20. K. S. Lim, M. H. Alves, L. A. Poole-Warren, P. J. Martens, Covalent incorporation of non-chemically modified gelatin into degradable PVA-tyramine hydrogels. *Biomaterials* **34**, 7097-7105 (2013).